


Adaptive Proxy-Based Controller of an Active Ankle Foot Orthosis to Assist Lower Limb Movements of Paretic Patients

Weiguang Huo^{†*}, Victor Arnez-Paniagua[‡],
Guangzheng Ding[‡], Yacine Amirat[‡] and
Samer Mohammed[‡]

[†]*Department of Mechanical Engineering, Imperial College London, UK*

[‡]*Laboratoire Images, Signaux et Systèmes Intelligents (LISSI), Université Paris-Est Créteil (UPEC), 94400 Vitry-sur-Seine, France. E-mails: victor.arnezpaniagua@univ-paris-est.fr; amirat@u-pec.fr; m201672442@hust.edu.cn; samer.mohammed@u-pec.fr*

(Accepted February 9, 2019. First published online: March 18, 2019)

SUMMARY

This paper deals with the control of an active ankle foot orthosis (AAFO) for paretic patients. State of the art methods using an AAFO try to track a predefined trajectory of the ankle joint while guaranteeing the wearer's safety in the presence of a large tracking error. Combining the wearer's safety and tracking accuracy is generally difficult to achieve at the same time, hence a trade-off should be found. Proxy-based sliding mode control (PSMC) offers great performances in both position tracking and safety guarantee. However, its tracking performance is subject to the influences of parameter uncertainties and external disturbances that generally occur during walking. This paper introduces an adaptation interaction method to the basic PSMC with an online adaptation of the proportional, integral and derivative parameters. At the same time, a gait phase-based ankle reference generation algorithm was proposed to adjust the joint reference trajectory in real time. The experiments using the AAFO show better tracking results with respect to basic PSMC while guaranteeing the safety.

KEYWORDS: Active ankle foot orthosis; Online reference generation; Adaptive PSMC; Wearable robot; Gait rehabilitation.

1. Introduction

Paretic patients generally present a limited movement of the ankle joint, which affects the life quality of the patient. This reduced mobility is produced by pathologies at the ankle joint that can be divided based on the direction of the movement. For example, in the dorsiflexion direction, foot drop and foot slap are common pathologies; the former is the inability to lift the tip of the foot during the swing phase of the gait and the latter is an uncontrolled landing of the toes following the heel strike.^{1,2} In the plantar flexion direction, a common affliction is the reduced push off power of the toes to prepare the leg for the swing phase. Such gait pathologies slow down the walking speed and increase the fall risk.

Ankle foot orthoses (AFO) have been designed to correct the abnormal gait pattern and can generally be classified into three categories: passive, semi-active, and active.³ In the early stages of the gait rehabilitation, the patient normally presents less voluntary movement at the ankle joint, which results in a higher requirement for direct assistance. On the contrary, a patient that can produce sufficient

* Corresponding author. E-mail: w.huo@imperial.ac.uk

ankle movement during walking could benefit more from a more compliant, semi-active device. For this reason, both active and semi-active orthosis are important in the integral rehabilitation process. In recent years, several active and semi-active ankle foot orthosis have been developed and different control strategies have been proposed to improve the benefits of active rehabilitation. Semi-active devices normally include an energy-storing element in the mechanical design to distribute the ankle joint energy in a desired pattern during the gait but are not able to introduce new sources of energy to assist the ankle joint. On the contrary, active ankle foot orthoses (AAFO) use direct actuation on the ankle joint. Examples of these devices are those that use series elastic actuators to produce the assistance torque,⁴⁻⁷ use electro-hydraulic actuation for both plantar and dorsiflexion assistance,⁸⁻¹¹ or do not use energy-storing elements but use DC motors instead.^{12,13}

The control strategies to determine the magnitude of the assistance provided by the orthoses can be roughly classified in four groups:^{3,6} (1) orthoses that apply a preselected assistance torque with respect to the detected gait phase,^{6,10,14,15} (2) devices that produce assistance as a function of electromyography (EMG) signals,^{9,16} (3) those that adapt the stiffness, inertia or impedance of the orthotic device based on the detected gait phase,^{4,17-19} or (4) orthoses provide assistance torque as a function of the error between the current ankle joint angle and a reference trajectory pattern commonly generated from healthy walking profiles.^{5,11,20-27} It is important for the AAFO to produce a smooth, continuous, and repeatable movement of the ankle joint in a clinical environment,²⁸ as the control method used for each exoskeleton has a direct impact on the level and rate of human adaptation to the active device.²⁹ The control challenges of an AAFO are mainly related to (i) a high nonlinearity of the AAFO; (ii) the human-robot transparency as the interaction dynamics between the human and the robot varies from one wearer to another, and (iii) important uncertainties related to the interaction with the wearer's voluntary movement and the external environment. In addition to the foregoing, intrinsic safety is very important for any rehabilitation robot that has a close interaction with patients.³⁰ A large position error may provoke a violent and thus unsafe response of the human-robot system and may cause physical damage to the wearer. Although there are various control methods that have been developed in the literature to control the AAFO, most of them are not able to guarantee both safety and high tracking accuracy. Sliding mode control (SMC) has gained much attention due to its design simplicity and robustness with respect to external disturbances.³¹ However, the well-known chattering side effect may excite high-frequency dynamics of the system and may produce a large control output. Adaptive control-based approaches are sufficiently robust with respect to uncertain disturbances, but the relative high controller gains may be harmful and risky for the wearer safety.³² Proxy-based sliding mode control (PSMC) introduced in ref. [33] efficiently combines the conventional SMC with PID control methods to increase the safety of the closed-loop system compared to the traditional PID control method. In other words, PSMC guarantees the safety when large tracking error occurs and ensures similar tracking performance during normal operation as that of the PID control. Since the AAFO system parameters and external disturbances vary from subject to subject, the fixed PID control parameters' values in PSMC limit its tracking and robustness performances. In ref. [34], the authors proposed a neural-network-based method to tune the PID parameters in PSMC and higher robustness was observed when implementing the method in a robotic orthosis for gait training conducted with healthy subjects.

This paper proposes a new adaptive proxy-based sliding mode control (APSMC) applied to the AAFO by introducing an adaptation interaction method,³⁵ which allows online tuning of the PID parameters in the PSMC scheme. Therefore, the proposed APSMC is able to adapt to the changes in the system's dynamics and external disturbances while providing a better tracking performance with respect to standard PSMC. Also, the benefit of safety is preserved. Furthermore, an online adaptive reference trajectory is proposed as a function of the walking speed of the wearer and the identification of the transitions between the different gait subphases. This adaptation of the reference trajectory avoids the use of a unique predefined trajectory of the ankle joint. It also allows the wearer focusing on the task and not on the synchronization with the reference trajectory.

The rest of this paper is organized as follows. Section 2 describes the human orthosis system. In Section 3, an online gait-phase-based gait reference generation algorithm is presented using the ground reaction forces. In Section 4, the APSMC control method is proposed and its stability is analyzed. Moreover, an experimental validation of the proposed method with two healthy subjects and two paretic patients is presented in Section 5. Finally, a discussion and conclusions are presented in Section 6.

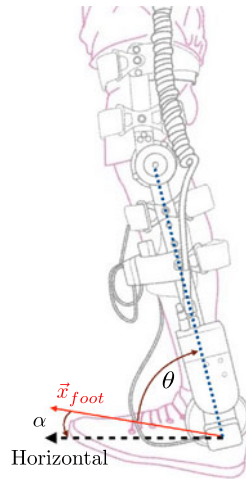


Fig. 1. The angles determining the foot and the shank orientations.

2. System Description

The orthosis used in this study is an actuated ankle foot orthosis attached to the subject’s left leg by means of straps to fix the orthosis to the calf and thigh, as shown in Fig. 1. The orthosis has one active and one passive degrees of freedom (DoF) at the ankle and knee joint levels, respectively. The AAFO is considered as rigidly fixed to the subject’s leg. The foot and the AAFO are considered as one unit referred to as the AAFO system. In this study, the problem of misalignment between the ankle joint and the AAFO’s rotational axis when donning the device has been considerably reduced by adjusting manually the orthosis to every wearer’s morphology using adaptable straps. A special care has been taken during experiments in order to avoid reaching of the full ankle joint flexion/extension which considerably reduce the joint misalignment.

In order to model the AAFO system, denote by θ the angle between the foot and the shank and by α the angle between the foot and the horizontal axis (Fig. 1). Only θ is measured using the embedded encoders in the AAFO.

The AAFO system’s dynamics can be expressed as the sum of internal and external torques affecting the ankle joint as follows:

$$J\ddot{\theta} = \tau_f + \tau_a + \tau_s + \tau_r + \tau_g + \tau_h + \tau \tag{1}$$

where J is the moment of inertia of the foot, τ_f is the solid and viscous friction torques, τ_a is the torque induced by the translational acceleration of the foot, τ_s is the system’s joint stiffness torque, τ_r is the torque induced by the ground reaction forces, τ_g is the gravity torque exerted by the foot on the ankle, τ_h is the torque produced by the plantar flexion and dorsiflexion muscle groups, and τ is the torque developed by the AAFO’s actuator. All the torques are considered positive if they induce a counterclockwise rotation. Furthermore, the torques and their rate of change are considered bounded.

Each of the aforementioned torques is defined as follows:

$$\begin{aligned} \tau_f &= -k_{f_s} \text{sgn}(\dot{\theta}) - k_{f_v} \dot{\theta} \\ \tau_a &= -k_a(a_y \cos \alpha - a_x \sin \alpha) \\ \tau_s &= -k_s(\theta - \theta_r) \\ \tau_r &= -k_r(x_g F_r) \cos \alpha \\ \tau_g &= -k_g \cos \alpha \end{aligned} \tag{2}$$

where k_{f_s} and k_{f_v} are the solid and viscous friction coefficients, k_s is the system’s stiffness coefficient, k_a is the system’s acceleration torque coefficient, a_x and a_y are the horizontal and vertical linear accelerations, k_r is the ground reaction force coefficient, F_r is the equivalent GRF applied to the center of mass of the foot, x_g is the distance of the center of mass from the ankle joint, and $k_g = mgx_g$ is the system’s gravity torque coefficient, where m and g represent the mass of the foot and the gravity acceleration coefficient. Replacing (2) in (1), we obtain the following:

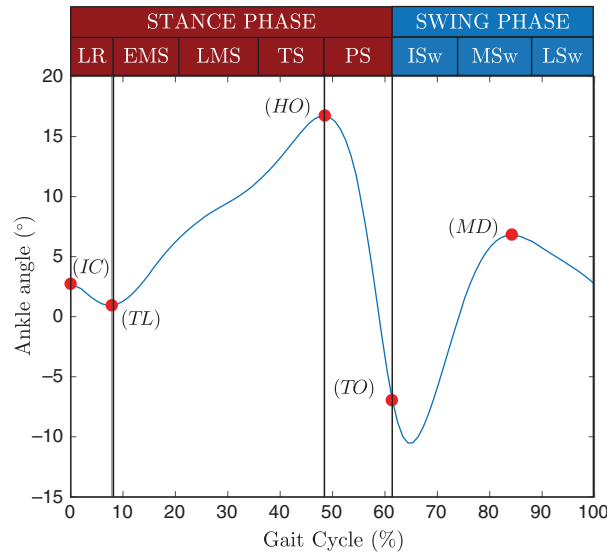


Fig. 2. The healthy ankle joint angle profile normalized to the gait cycle. The gait cycle is divided in the subphases and the gait events are marked.

$$\begin{aligned}
 J\ddot{\theta} + k_f\dot{\theta} + k_s\theta &= -k_g \cos \alpha - k_{f_s} \operatorname{sgn}(\dot{\theta}) + k_s\theta_r \\
 &\quad - k_a(a_y \cos \alpha - a_x \sin \alpha) \\
 &\quad - k_r(x_g F_r) \cos \alpha + \tau_h + \tau
 \end{aligned} \tag{3}$$

The system internal and external torques are considered as disturbances to the system. Therefore, (3) can be rewritten as follows:

$$J\ddot{\theta} + B\dot{\theta} + K\theta = \tau + d, \tag{4}$$

with

$$\begin{aligned}
 d &= -k_g \cos \alpha - k_{f_s} \operatorname{sgn}(\dot{\theta}) + k_s\theta_r \\
 &\quad - k_a(a_y \cos \alpha - a_x \sin \alpha) - k_r(x_g F_r) \cos \alpha + \tau_h
 \end{aligned} \tag{5}$$

where d represents all the nonlinear disturbances, $B = k_{f_v}$, and $K = k_s$.

3. Online Reference Gait Generation

In order to control the AAFO system, a reference trajectory that represents the healthy ankle joint profile during the gait is required. To produce this reference, a motion capture system (Motion Analysis Corporation, Santa Rosa, CA, USA, six cameras, Sampling Frequency 100 Hz) and two force plates (AMTI, Watertown, MA, USA, Sampling Frequency 1000 Hz) were used to measure the normal gait of 20 healthy participants and calculate the average profile. For more details on this capture system, refer to ref. [36]. However, it is important to synchronize the reference used for the controller to the wearer’s gait. For this purpose, two technics are mostly used: (1) to repeatedly generate the healthy ankle joint profile with a time-fixed periodicity, and use an audible or visual cue for the wearer to synchronize, or (2) to adapt in real time the reference to the wearer’s walking speed. For this study, an adaptive reference is considered and the method to generate it is described in the following.

3.1. Gait phases

The gait cycle can be divided into stance and swing phases, as shown in Fig. 2. To analyze the stance phase, it is further divided into the following subphases that are defined by the interaction of the feet with the ground: loading response (LR), early-mid-stance (EMS), late-mid-stance (LMS), terminal stance (TS), and pre-swing (PS). The swing phase is also divided based on the position of the foot relative to the opposite foot. These subphases are as follows: initial swing (ISw), mid-swing (MSw),

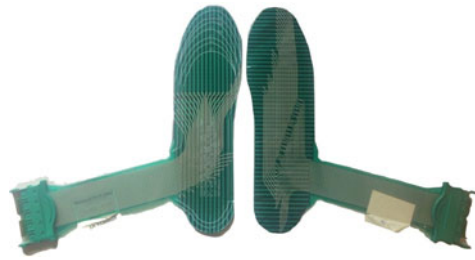


Fig. 3. The Tekscan FSR insole.

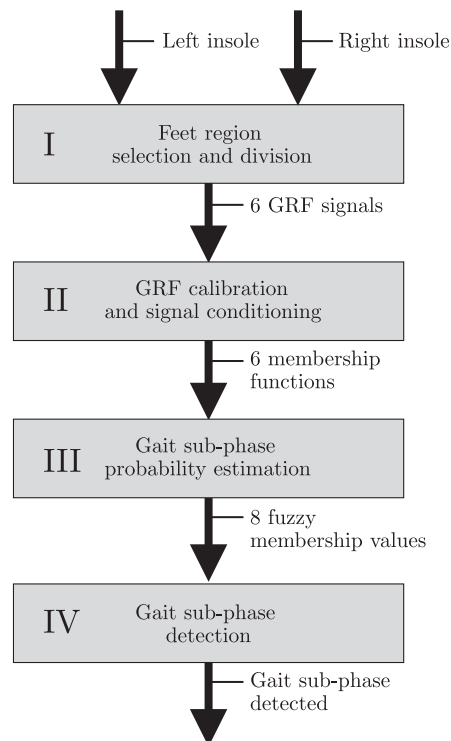


Fig. 4. The algorithm to detect the gait subphases based on the signals from the insoles embedded with force sensitive resistor matrices.

and terminal swing (TSw). Therefore, the transition between the stance subphases is triggered by specific events during the gait, such as initial contact (IC), toe landing (TL), heel off (HO), and toe off (TO). During the swing phase, the maximum dorsiflexion (MD) can be identified. Also, the gait event during the stance phase occurs at the moments when the ankle joint angle profile switches from dorsiflexion to plantar-flexion and vice versa, as shown in Fig. 2.

3.2. Gait phase detection

In order to detect the gait events, a force-sensitive resistor matrix (FSRM) embedded in each insole (Tekscan Co.) is used to measure the interaction between the feet and the ground, as shown in Fig. 3. The algorithm to detect the gait subphases is described in four blocks, as shown in Fig. 4, and is presented as follows. The measured surface of each insole is divided into three regions: the heel, the mid foot, and the toes areas. Then, the summary of all the FSRM nodes for each region is calculated as described in block I.

In block II, the six signals from the different areas of the feet are calibrated by detecting the minimum and maximum values from the beginning of the session.

$$r_j = \max(\vec{F}_{ij}) - \min(\vec{F}_{ij}) \quad (6)$$

Table I. Fuzzy rules for gait phase detection. \mathcal{F}_{ij} with $j \in \{1, \dots, 6\}$ are the membership functions for each foot regions of both insoles. μ_i represents the fuzzy variable that gives the probability for each subphase $i \in \{1, \dots, 8\}$.

\mathcal{F}_{i1}	$\max(\mathcal{F}_{i2}, \mathcal{F}_{i3})$	\mathcal{F}_{i4}	\mathcal{F}_{i5}	\mathcal{F}_{i6}	μ_i
Large	Small	Small	N/A	Large	μ_{LR}
Large	Small	Small	N/A	Small	μ_{EMS}
Large	Large	Small	N/A	Small	μ_{LMS}
Small	Large	Small	N/A	Small	μ_{TS}
N/A	Large	Large	N/A	N/A	μ_{PS}
Small	Small	Large	N/A	N/A	μ_{ISw}
Small	Small	Small	Large	N/A	μ_{MSw}
Small	Small	Small	N/A	Large	μ_{TSw}

where r_j contains the range of the measured values of each foot region j , and \vec{F}_{ij} is a vector containing all the values of the foot region j from the beginning of the session until a given time t . Then, the threshold value for each foot region (T_j) is given by

$$T_j = r_j \cdot h + \min(\vec{F}_{ij}) \tag{7}$$

where h is the threshold percentage. An empirical value of 5% was found to be effective ($h = 0.05$). A Mamdani fuzzy inference system¹⁵ is used to calculate the probability of each subphase at any given time. The membership function \mathcal{F} for each sensor j at any given time t is given by

$$\mathcal{F}_{ij} = \frac{1}{2} \left(\tanh \left(\frac{k_j(F_{ij} - T_j)}{r_j} - 1 \right) + 1 \right) \tag{8}$$

where k_j is the gain for each foot region j , and F_{ij} is the measurement output of each foot region j at a given time t during the session. Effective values for k_j were empirically tuned and were set to $k_{1,2,3} = 3$ and $k_{4,5,6} = 4$. This was done by increasing k_j of each membership function \mathcal{F}_{ij} until every gait phase could be detected during level walking done by the subject.

The rules that define each subphase’s probability are described in Table I, where μ_{LR} , μ_{EMS} , μ_{LMS} , μ_{TS} , μ_{PS} , μ_{ISw} , μ_{MSw} , and μ_{TSw} correspond to the occurrence likelihood for the loading response, early mid-stance, late mid-stance, terminal stance, pre-swing, initial swing, mid-swing, and terminal swing subphases, respectively. In block III, the fuzzy membership value FMV is calculated for each subphase as follows:

$$\begin{aligned} \mu_{LR} &= \min(\mathcal{F}_{i1}, 1 - \max(\mathcal{F}_{i2}, \mathcal{F}_{i3}), 1 - \mathcal{F}_{i4}, \mathcal{F}_{i6}) \\ \mu_{EMS} &= \min(\mathcal{F}_{i1}, 1 - \max(\mathcal{F}_{i2}, \mathcal{F}_{i3}), 1 - \mathcal{F}_{i4}, 1 - \mathcal{F}_{i6}) \\ \mu_{LMS} &= \min(\mathcal{F}_{i1}, \max(\mathcal{F}_{i2}, \mathcal{F}_{i3}), 1 - \mathcal{F}_{i4}, 1 - \mathcal{F}_{i6}) \\ \mu_{TS} &= \min(1 - \mathcal{F}_{i1}, \max(\mathcal{F}_{i2}, \mathcal{F}_{i3}), 1 - \mathcal{F}_{i4}, 1 - \mathcal{F}_{i6}) \\ \mu_{PS} &= \min(\mathcal{F}_{i1}, \mathcal{F}_{i4}) \\ \mu_{ISw} &= \min(1 - \mathcal{F}_{i1}, 1 - \max(\mathcal{F}_{i2}, \mathcal{F}_{i3}), \mathcal{F}_{i4}) \\ \mu_{MSw} &= \min(1 - \mathcal{F}_{i1}, 1 - \max(\mathcal{F}_{i2}, \mathcal{F}_{i3}), 1 - \mathcal{F}_{i4}, \mathcal{F}_{i5}) \\ \mu_{TSw} &= \min(1 - \mathcal{F}_{i1}, 1 - \max(\mathcal{F}_{i2}, \mathcal{F}_{i3}), 1 - \mathcal{F}_{i4}, \mathcal{F}_{i6}) \end{aligned} \tag{9}$$

Finally, in block IV, the subphase with the maximum FMV value is selected. By calculating the duration of each subphase and the duration of each step, it is possible to calculate in real time the duration percentage of each subphase with respect to the gait cycle, and the time between the gait events. At every new detection of a gait subphase, the average duration percentage for each subphase is calculated from the last five steps. The gait duration is then updated eight times per gait cycle, one time per subphase detected. The average duration percentage of each subphase is obtained after the first five steps and is then updated after each subphase detection.

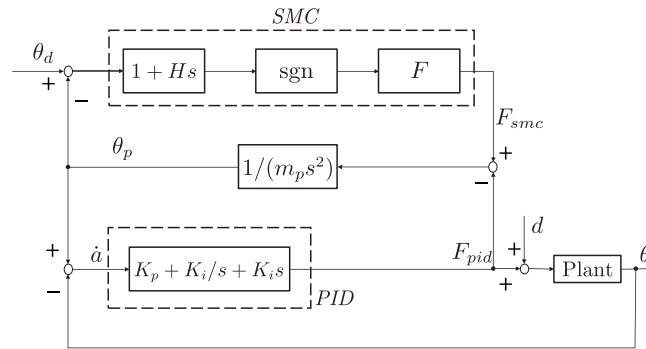


Fig. 5. Structure of the conventional PSMC control.

3.3. Adaptive reference generation

The adaptive reference trajectory is calculated by connecting the ankle joint angle values at the gait events defined above using a cubic spline function. For example, if the TL event is detected, a cubic spline trajectory that connects the current value of the ankle joint angle reference to the HO event ankle joint angle value is calculated. The duration of the cubic spline is defined by the measured gait duration. The adaptive reference of the ankle joint angular velocity and accelerations are calculated afterwards by numerically deriving the cubic spline trajectory. For the swing phase, if the TO event is detected, the cubic spline is calculated from the current ankle joint angle reference, then follows the MD key point in the middle of the path, and ends with the IC event.

4. Adaptive Proxy-based Controller

4.1. APSMC structure

The PSMC control structure proposed in ref. [37] is depicted in Fig. 5. A virtual object, referred as proxy, was used to connect a first-order SMC and a conventional PID controller. The advantage of the PSMC control structure is that an over-damping motion can be obtained to avoid large actuator torque when a large position error occurs and a relatively accurate tracking performance can be guaranteed by the inner PID controller. To further improve the robustness of the traditional PSMC with respect to disturbances from the wearer or the environment, an adaptive tuning algorithm is introduced to tune the parameters of the inner PID controller. The whole structure of the proposed APSMC is shown in Fig. 6.

The SMC controller shown in Fig. 6 is designed as follows:

$$\tau_{SMC} = F \text{sgn}(e_\sigma + H \dot{e}_\sigma) \tag{10}$$

with

$$e_\sigma = \theta_d - \theta_p \tag{11}$$

where $H > 0$ and $F > 0$ denote scalar design parameters, θ_d and θ_p represent the desired ankle angle and the proxy angle, respectively.

The adaptive PID controller is designed as follows:

$$\tau_{PID} = K_p e_p + K_i \int_0^t e_p dt + K_d \dot{e}_p \tag{12}$$

with

$$e_p = \theta_p - \theta \tag{13}$$

where θ shows the real ankle angle. K_p , K_i , and K_d denote the adaptive proportional, integral, and differential parameters, respectively.

By defining

$$a = \int_0^t (\theta_p - \theta) d\tau \tag{14}$$

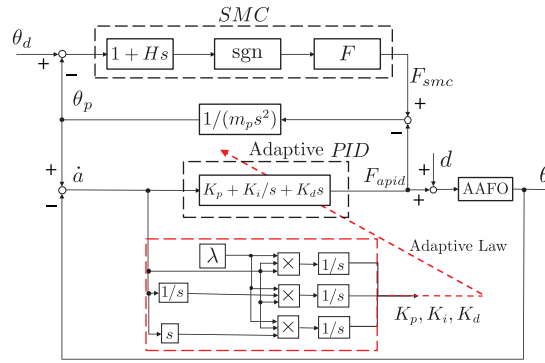


Fig. 6. Structure of the proposed APSMC control.

and

$$\sigma = \theta_d - \theta + H(\dot{\theta}_d - \dot{\theta}) \tag{15}$$

the SMC (10) and adaptive PID (12) controllers can be re-expressed as follows:

$$F_{SMC} = F \operatorname{sgn}(\sigma - \dot{a} - H\ddot{a}) \tag{16}$$

and

$$F_{PID} = K_p \dot{a} + K_i a + K_d \ddot{a} \tag{17}$$

According to the analysis in ref. [37], The dynamics of the proxy (see Fig. 5) can then be modeled as follows:

$$m_p \ddot{\theta}_p = \tau_{SMC} - \tau_{PID} \tag{18}$$

where m_p is the proxy mass which is set to zero. Then, we have

$$\tau_{SMC} = \tau_{PID} = \tau \tag{19}$$

By applying the relationship between the signum function $\operatorname{sgn}()$ and the saturation function $\operatorname{sat}()$, we have

$$y + X = Y \operatorname{sgn}(z - Zy) \Leftrightarrow y = -X + Y \operatorname{sat}\left(\frac{z/Z + X}{Y}\right) \tag{20}$$

where $Y, Z > 0$ and $X, y, z \in R$.

Therefore, the whole control law can be rewritten as follows:

$$\tau = F \operatorname{sat}\left(\frac{K_d}{F} \left(\frac{\sigma - \dot{a}}{H} + \frac{K_p \dot{a} + K_i a}{K_d}\right)\right) \tag{21}$$

with

$$\ddot{a} = -\frac{K_p \dot{a} + K_i a}{K_d} + \frac{F}{K_d} \operatorname{sat}\left(\frac{K_d}{F} \left(\frac{\sigma - \dot{a}}{H} + \frac{K_p \dot{a} + K_i a}{K_d}\right)\right) \tag{22}$$

4.2. Adaptive tuning algorithm

During walking with the assistance of the AAFO, the parameters of model (3) are different for each individual and the ankle joint stiffness varies. Moreover, the human-AAFO is subject to disturbances such as the GRF which is varying with gait phases. To deal with these issues, an online tuning PID controller is used. Leading up to the application of the adaptation interaction theory to the inner PID controller (see Fig. 6), the inner PID-based human-AAFO closed-loop system is divided into four independent subsystems: the proportional part, integral part, derivative part, and the human-AAFO system (see Fig. 7). The PID parameters, $\beta = \{K_p, K_i, K_d\}$, are considered as the connection weights between subsystems. Based on the adaptive interaction theory presented in ref. [38], the turning of

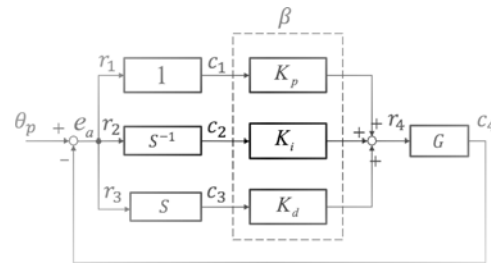


Fig. 7. PID subsystem interaction. G denotes the human–exoskeleton system.

the PID parameters β can be considered as a minimum problem and associated performance index \mathcal{E} is designed as follows:

$$\mathcal{E} = e_a^2 = (\theta_p - c_4)^2 \tag{23}$$

where $c_4 = \theta$ shows the output of the fourth subsystem, that is, the human–AAFO system.

According to the analysis shown in ref. [38], \mathcal{E} monotonically decreases with time, if the connection weight β is adapted as

$$\dot{\beta} = -\gamma \frac{d\mathcal{E}}{d\beta} \tag{24}$$

with $\gamma > 0$,

Applying (24) to the online tuning of the PID parameters, we have

$$\dot{\beta} = -\gamma \frac{d\mathcal{E}}{de_a} \circ G'(\tau_{\text{PID}}) \circ y_i \tag{25}$$

where $y_i, i \in \{1, 2, 3\}$ shows the input of each subsystem as shown in Fig. 7. $G'(\tau_{\text{PID}})$ represents the Frechet derivative of the human–exoskeleton system model G (i.e., the model (4)) with input $\tau = \tau_{\text{PID}}$ and output θ .

From (17) and (25), the online tuning algorithm of the PID parameters is given by

$$\begin{aligned} \dot{K}_p &= -\gamma \frac{d\mathcal{E}}{de_a} \circ G'(\tau_{\text{PID}}) \circ \dot{a} \\ \dot{K}_i &= -\gamma \frac{d\mathcal{E}}{de_a} \circ G'(\tau_{\text{PID}}) \circ a \\ \dot{K}_d &= -\gamma \frac{d\mathcal{E}}{de_a} \circ G'(\tau_{\text{PID}}) \circ \ddot{a} \end{aligned} \tag{26}$$

According to approximation tuning method proposed in ref. [39], the Frechet derivative for the second-order system, for example, G , can be further simplified as

$$G'(\tau_{\text{PID}}) \circ y_i = ky_i \tag{27}$$

where k is a constant. Thus, (26) becomes

$$\begin{cases} \dot{K}_p = 2\gamma ke_a \dot{a} \\ \dot{K}_i = 2\gamma ke_a a \\ \dot{K}_d = 2\gamma ke_a \ddot{a} \end{cases} \tag{28}$$

Since $e_a = \theta_p - \theta = \dot{a}$, (28) can be further rewritten as

$$\begin{cases} \dot{K}_p = \lambda \dot{a} \\ \dot{K}_i = \lambda a \\ \dot{K}_d = \lambda \ddot{a} \end{cases} \tag{29}$$

where $\lambda = 2\gamma k$.



Fig. 8. A parietic patient wearing the ankle joint exoskeleton and the FSR sensors.

It should be noted that using the approximation tuning method (29), \dot{K}_p is always positive when the error a is not zero. Hence, the upper limit of the K_p should be limited in practice.

4.3. Stability analysis

Define the tracking error $e = \theta_d - \theta$ and the error vector as

$$E = [e \quad E_1] \quad (30)$$

where $E_1 = [\dot{e} \quad \dot{a}]$. By substituting $e = \theta_d - \theta$ to (4), the error dynamics equation is obtained as follows:

$$J\ddot{e} + B\dot{e} + Ke = -\tau + \varphi \quad (31)$$

with

$$\varphi = J\ddot{\theta}_d + B\dot{\theta}_d + K\theta_d - d \quad (32)$$

where $|\varphi| \leq \delta_0$ with $\delta_0 > 0$. To demonstrate the stability of the APSMC for the system (4), the following proposition is introduced.

Proposition: Considering the closed-loop system composed of system (4) and an APSMC controller, that is, (21), (22), and (29), the PID parameter values are appropriately chosen. Then, there exists a closed set ξ including the origin with which $E \rightarrow \xi$ is achieved as $t \rightarrow \infty$.

The stability of the PSMC controller is proved in ref. [37]. Indeed, the human–exoskeleton system can be considered as a special case (i.e., a single-joint case) in ref. [37]. The online tuning algorithm (29) is also able to obtain appropriate parameter values for the PID controller designed for a second-order nonlinear system (e.g., the human–exoskeleton system), which has been proven in ref. [40]. For more details, refer to refs. [37] and [40].

5. Experimental Evaluation

5.1. Experimental setup

Figure 8 shows a parietic patient wearing the AAFO. The AAFO is driven by a DC motor (Maxon, Switzerland) with gear transmission. The maximum output torque of the AAFO is 15 Nm. The AAFO is equipped with an incremental encoder that measures the angle θ between the foot and the shank and angular velocity $\dot{\theta}$ is derived numerically. The motion range of the AAFO is from 1.171 rad (dorsiflexion) to 2.14 rad (plantar flexion). The AAFO is controlled using a myRio-1900 card (NI, USA). At the same time, two FSRM sensors (Tekscan, USA) are used to measure the GRF used for gait phase detection. The GRF data are acquired with 100 Hz and sent to a Hub as shown in Fig. 8. Both the AAFO and the FSR Hub are connected to a host PC using Wi-Fi. The control algorithm is running in LabView on the host PC, in which the data from the AAFO and the FSR sensors are synchronized.

Table II. Subjects' information.

	Subjects	Sex	Age	Height (cm)	Weight (kg)
Healthy	1	Male	31	180	78
	2	Male	31	170	76
Patient	1	Male	24	181	63
	2	Male	58	176	79

5.2. Experimental protocol

To evaluate the performance of the proposed APSMC, three experiments were carried out. The first experiment is aimed to compare the tracking performance of the proposed APSMC to that of the conventional PSMC, and the second experiment is designed to show the effectiveness of the proposed method in assisting the paretic patients during walking. Finally, the compliance of the APSMC was evaluated.

Two healthy subjects (see Table II) participated in the first experiments and were asked to simulate abnormal gaits (i.e., fixing the knee joint) during walking on a treadmill with the AAFO and sensors shown in Fig. 8 under three conditions: *without assistance*, *with PSMC control*, and *with APSMC control*. During each condition, the subjects were asked to walk for 80 s with a low walking speed (≈ 0.39 m/s). The parameters for PSMC are set as $K_p = 7$, $K_i = 1$, $K_d = 0.5$, while the H is set based on the gait phases, that is, $H = 0.01$ during swing phase and $H = 0.2$ during stance phase. The same PID control parameter values are also used as the initial values of the adaptive PID control parameters in the APSMC, and the adaptive gain is set as $\gamma = 20$.

During the second experiment, two paretic patients (see Table II) were asked to perform the over-ground walking while wearing the AAFO on their affected legs (left legs for both patients) under two conditions: *without assistance*, and *with APSMC control*. The same parameter values of the APSMC used during the first experiment were also used.

In order to evaluate the compliance of the foot-AAFO system by using the proposed APSMC controller, experiments of tracking a step input of joint angle with an amplitude of 1.8 rad were carried out when a healthy subject sat on a chair while wearing the AAFO. The step input was used to simulate the large tracking error.

5.3. Experimental results

Figure 9(a) and (b) show, respectively, the generated reference angles and two healthy subjects' average ankle joint angles without assistance. It can be observed that the simulated ankle joint angles of the two subjects are significantly different from the references which are close to that of the healthy gaits as shown in ref. [36]. Using the conventional PSMC, the subjects' ankle angles are assisted to be close to the references (see Fig. 9(c) and (d)). The errors between the subjects' ankle angles and the references can be further reduced using the proposed APSMC control method. Figure 10 shows the root-mean-square-errors (RMSE) between the two subjects' ankle angles and the references during the three conditions (without assistance: Subject 1, 4.3 ± 5.6 , Subject 2, 4.1 ± 5.2 ; with PSMC: Subject 1, 2.8 ± 4.4 , Subject 2, 3.1 ± 4.0 ; with APSMC: Subject 1, 2.0 ± 2.9 , Subject 2, 2.1 ± 2.9 , unit: degrees). The tracking errors using the APSMC can be reduced by $\approx 28.6\%$ and $\approx 32.3\%$ for the two subjects compared to the ones using PSMC.

It should be noted that the references shown in Fig. 9 were separately generated based on the measured group reaction forces during each condition for two subjects. Figure 11(a) presents the experimental results measured with Subject 1 using the proposed APSMC, such as the ankle angles, ankle velocities, tracking error, detected gait phases and changes of the PID parameters' values. All phases mentioned in Section 3.1 can be clearly detected and the gait-phase based reference angles show the similar profile among different gait cycles. Regarding the performance of adaptive algorithm of the PID parameters, one can observe that the tracking error during the last 30 s (RMSE: 2.01 deg) are much lower than during the first 20 s (RMSE: 4.01 deg) [see Fig. 11(a)]. Correspondingly, significant changes can be observed in the three PID parameters' values in the first 20 s. As analyzed in Section 4.2, the proportional parameter K_p always increase unless the tracking error converges to zero, which is difficult to be guaranteed in practice. Hence, an upper limitation is used as shown in Fig. 11(b). Here, the upper limitation was selected using a trial-and-error method to ensure the stability of the closed-loop system as well as a sufficient tracking accuracy.

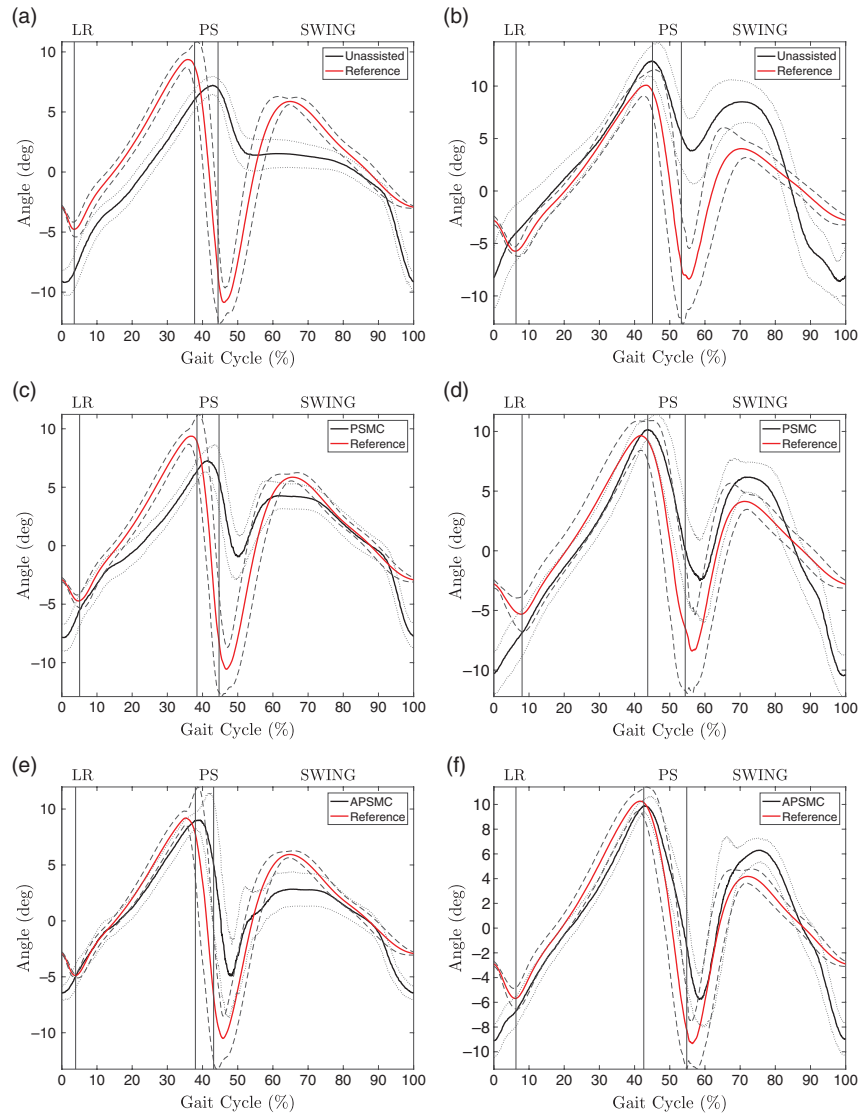


Fig. 9. Average ankle joint trajectories and related standard deviations (dash lines) measured under three conditions: without assistance, with PSMC control, and with APSMC control. (a) Subject 1: without assistance; (b) Subject 2: without assistance; (c) Subject 1: PSMC; (d) Subject 2: PSMC; (e) Subject 1: APSMC; (f) Subject 2: APSMC.

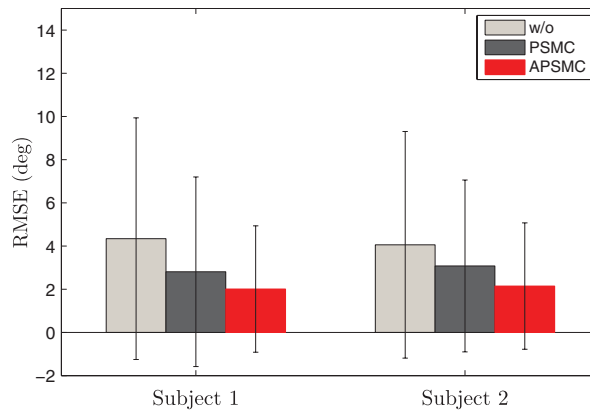


Fig. 10. The measured RMSE during three conditions: without assistance (w/o), with PSMC, and with APSMC.

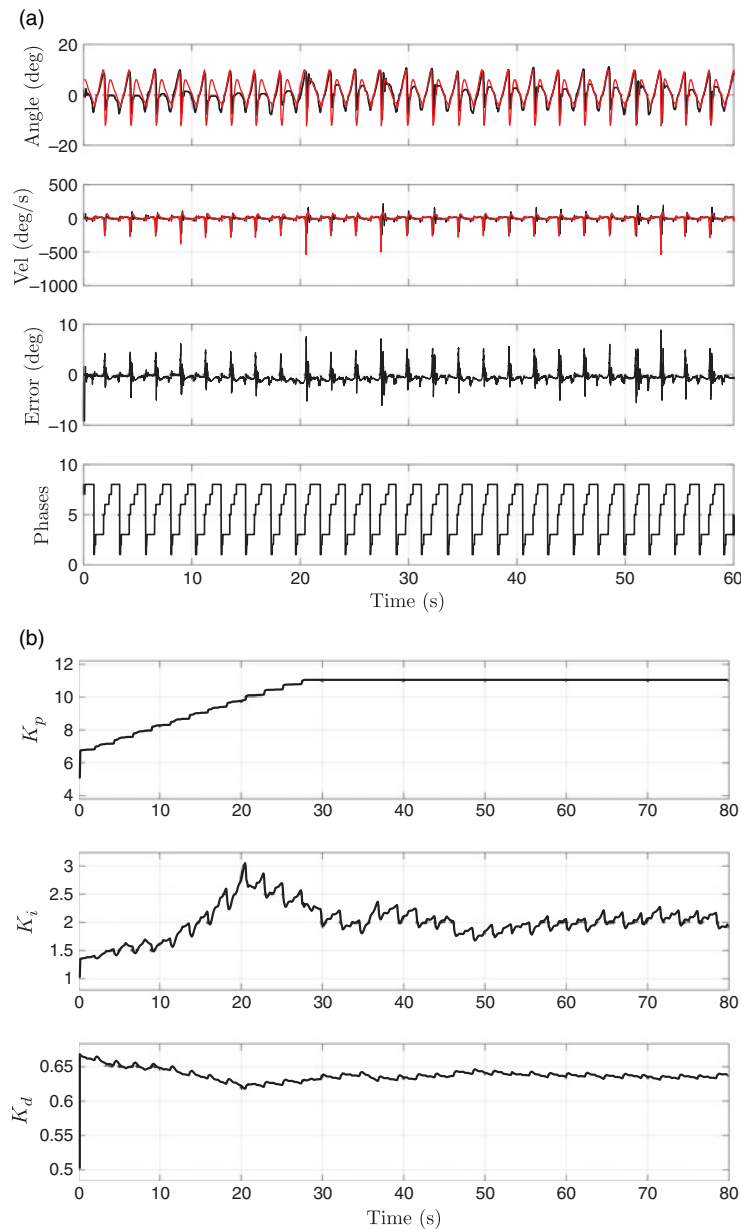


Fig. 11. Experimental results with subject 1. (a) The ankle angles (red line: reference; black line: measured), ankle velocities (red line: reference; black line: measured), tracking error, and detected gait phases (1:LR; 2:EMS; 3:LMS; 4:TS; 5:PS; 6:ISw; 7:MSw; 8:LSw). (b) The changes of the PID parameters' values.

Figure 12 shows the average ankle angles measured with the paretic patients during two conditions: without assistance and with APSMC. It is shown that patient 1 presents an over-dorsiflexed ankle joint profile, while patient 2 shows an insufficient dorsiflexion throughout the gait cycle. The ankle joint trajectory, velocity, and detected gait phases when the patients were assisted using APSMC method are presented in Fig. 13(a) and (b), and the changes of the PID parameters' values in Fig. 13(c) and (d). Although some abnormal gait-phase sequences were performed by the patients during some steps (see Fig. 13(a)), the generated ankle references are not affected.

Some important kinematic features, such as the average range of motions (ROMs) during push off and swing phase, the average peak plantar flexion and dorsiflexion angles during push off, and the average peak dorsiflexion angle during swing phase (see Fig. 12), were analyzed and shown in Fig. 14. For patient 1, a limited ankle joint ROM during push-off was performed during the unassisted session, which leads to an insufficient plantar flexion angle at the end of the push-off motion. Note that the peak dorsiflexion angle at the end of the stance phase without assistance is similar to that with

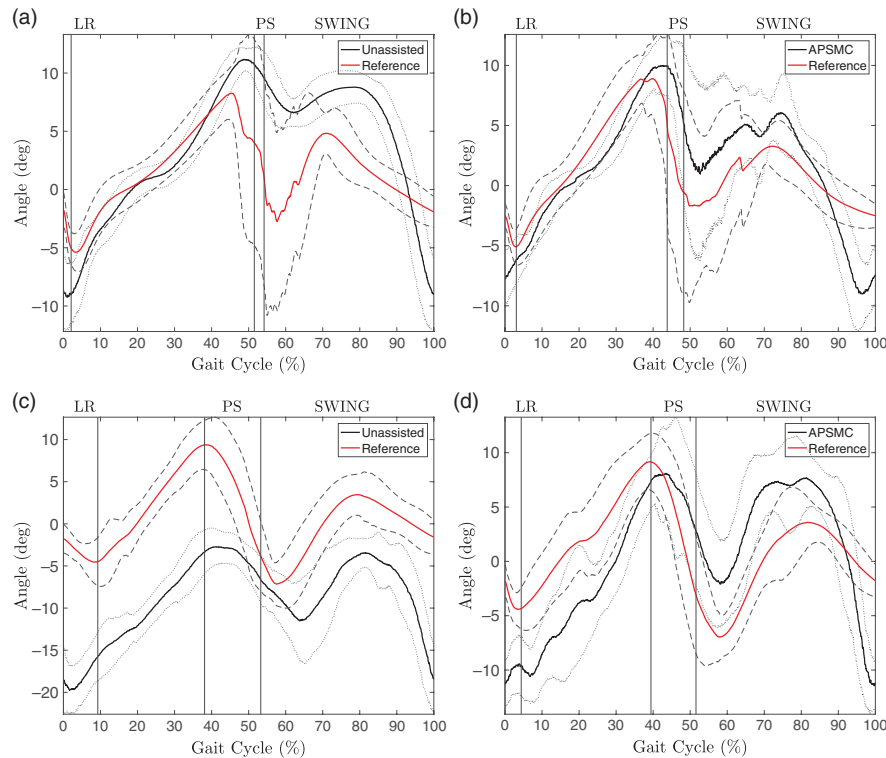


Fig. 12. The patients' average ankle joint trajectories measured under two conditions: without assistance and with APSMC control. The red lines represent the reference trajectory and black lines are the ankle joint angles produced by the patient. The gray dotted and slashed lines show the standard deviation for the unassisted and assisted sessions, respectively. All figures are normalized with respect to the gait cycle. (a) Patient 1: No assistance; (b) Patient 1: APSMC; (c) Patient 2: No assistance; (d) Patient 2: APSMC.

assistance, but a higher plantar flexion angle at the end of push-off motion can be observed when the assistance is provided. Hence, the patient's ankle joint push-off ROM can be significantly increased by 96.3% with assistance. Similarly, there exists a significant increase (by 130.1%) of the ankle joint ROM during the swing phase. Patient 2 presented an insufficiently dorsiflexed ankle joint profile (see Fig. 12). The ankle joint ROM during push-off was increased by 13% when the assistance was provided. Moreover, the dorsiflexion angle was increased by 11.9° during swing phase (from -2.8° to 9.1°), which effectively compensates for the drop foot pathology (with a 32.5% increase in the ankle joint ROM during the swing phase).

Regarding the gait phase detection accuracy, the fuzzy logic based algorithm showed a 99% correct detection rate during the experiments with healthy subjects. In the experiments with the paretic patients, this performance was reduced to 82% for patient 1, and 92% for patient 2. The reduction of accuracy could be due to the pathological gaits of the patients that produced different gait patterns, for example, if the patient lands the foot on the ground with a flat foot instead with the heel, then the first gait subphase would be skipped and, therefore, not detected by the algorithm. However, it should be noted that the reference trajectory was designed to remain bounded and safely converged to the desired profile after the next gait subphase was correctly detected (see Fig. 13(a) and (b)). Moreover, since the gait phases are detected by measuring the ground reaction force using two insoles embedded with force sensitive resistor matrices (see Fig. 3), the gait phases can be quickly detected with appropriate threshold values for the fuzzy logic based detection algorithm.

5.4. Compliance performance

To compare the performances of the propose method with those of a PID control, a trial-and-error method was used for tuning the PID parameters to $K_p = 9$, $K_i = 2$, $K_d = 1$. To guarantee similar experimental conditions, the same values of these parameters in PID control are set as the initial values of the adaptive proportional, integral and derivative parameters in APSMC. The adaptive gain γ is set to 20. Three trials were performed with different values of H : $H = 0.5, 0.2, 0.1$. The ankle

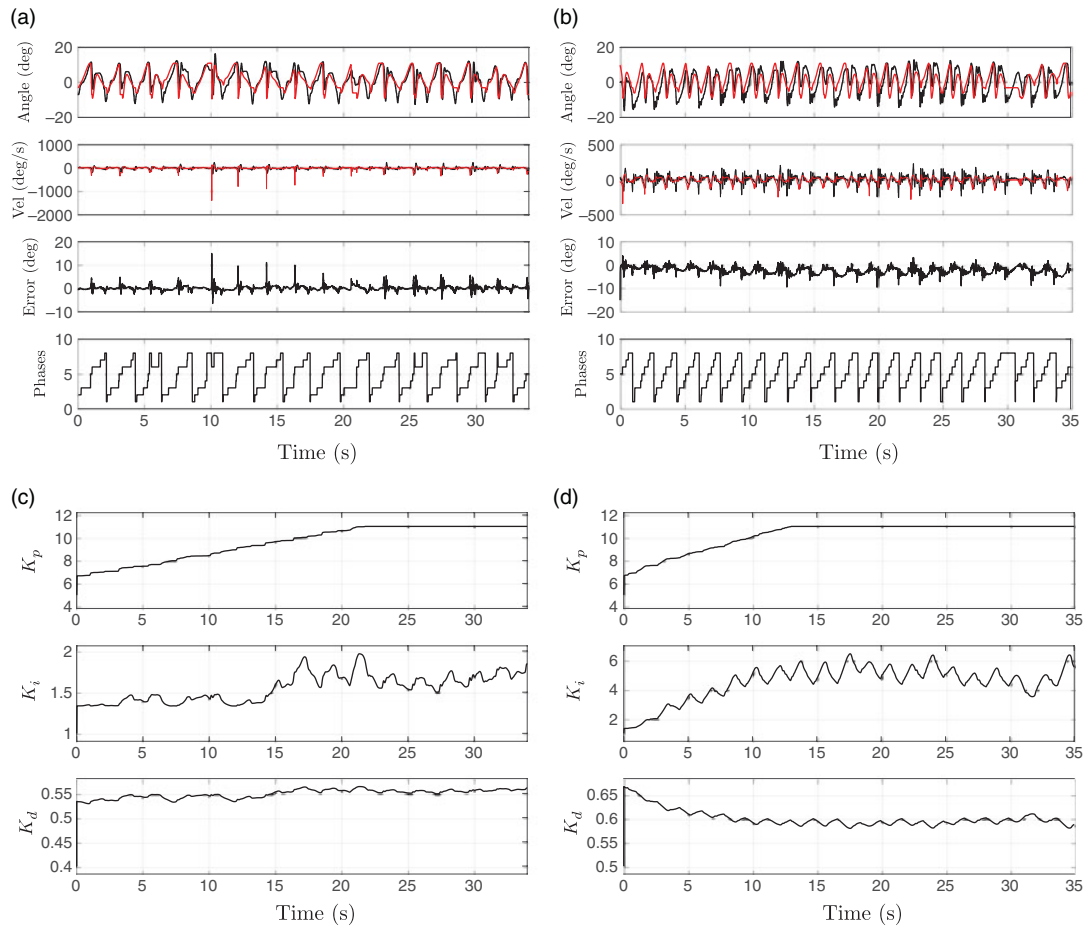


Fig. 13. Experimental results with the paretic patients. (a) and (b) The ankle angles (red line: reference; black line: measured), ankle velocities (red line: reference; black line: measured), tracking error, and detected gait phases (1:LR; 2:EMS; 3:LMS; 4:TS; 5:PS; 6:ISw; 7:MSw; 8:LSw). (a) Patient 1: Results; (b) Patient 2: Results; (c) Patient 1: Adaptive parameters; (d) Patient 2: Adaptive parameters.

angle and angular velocity are shown in Fig. 15. The results show that with a reasonable high value of H , the system using APSMC achieves a smooth, slow, and safe tracking toward the desired value. The smaller the H , the faster the tracking speed. With a very small H , APSMC behaves closer to the PID controller. Thus, with an appropriate value of H , the APSMC ensures the compliance of the system, while PID has a relative abrupt response to a high tracking error. Although small K_p or large K_d can also increase the damping of the close-loop system, this cannot ensure the accurate tracking performance when the tracking errors are relatively small, as discussed in Section 5.3.

6. Discussion and Conclusion

6.1. Discussion

Compared to the Frechet tuning algorithm³⁸, a common method for tuning PID controller, an advantage of the use of approximation tuning algorithm (28) is that the human-exoskeleton model is not required. However, as analyzed in Section 4.2, an upper limitation of the proportional parameter K_p is needed to ensure the stability of the closed-loop system if there always exists a tracking error, which is inevitable in practice. Moreover, one can observe that only one parameter is used for tuning the PID controller using the approximation tuning algorithm, which makes it easier to use compared to other existing methods such as fuzzy-based approaches, for example, ref. [41] and neural network based ones, for example, ref. [34].

Furthermore, various adaptive algorithms have also been proposed to online tune the system parameters for model-based control methods^{11,27,42}. It will be interesting to integrate these adaptive

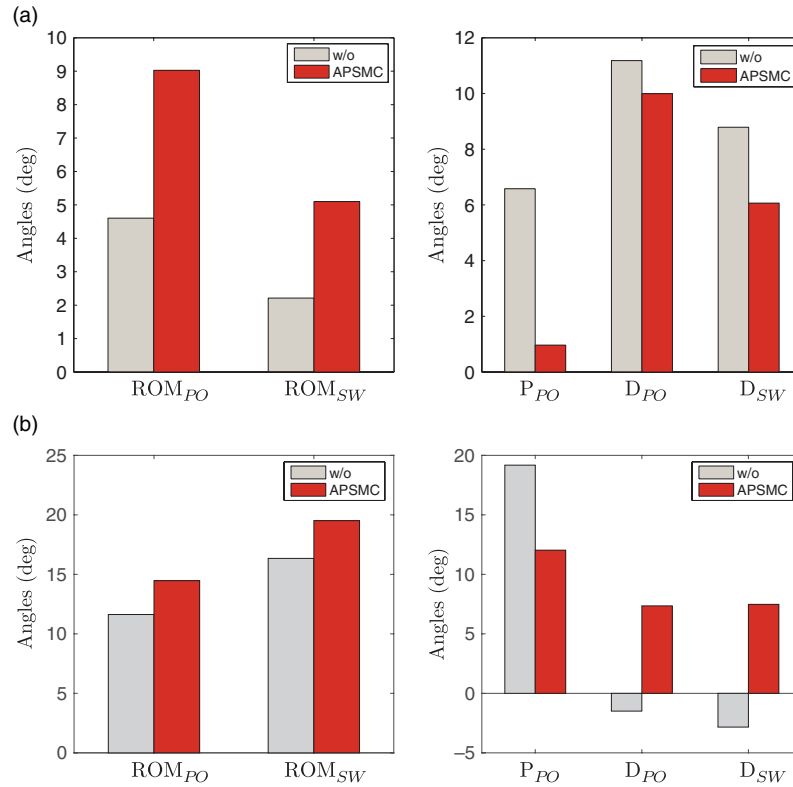


Fig. 14. The changes of the main walking kinematic features of the paretic patient from the condition “without assistance (w/o)” to the condition “with assistance (APSMC). (PO : Push off moment; SW : Swing phase, ROM: Range of Motion, P: Planter flexion, D: Dorsiflexion). (a) Patient 1 and (b) Patient 2.

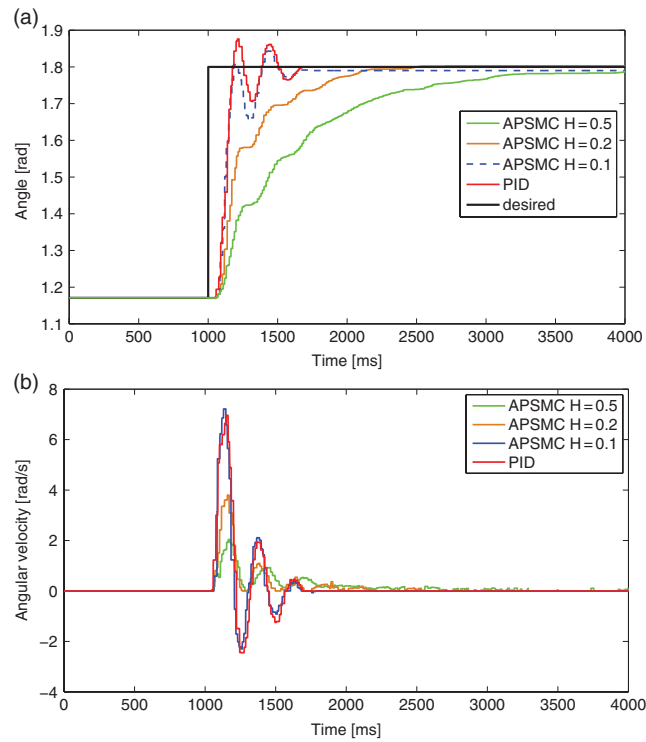


Fig. 15. Safety tests using PID and APSMC. (a) Step wave tracking which simulates the big error occurs. (b) Angular velocity during the tracking process.

algorithms with PSMC control structure since the PSMC structure can be further extended to take into account the system model according to the signum function (20) used for the PSMC design.

6.2. Conclusion

This paper proposes a new APSMC for tracking control of an AAFO during walking activity. APSMC is achieved by introducing a suitable adaptation of the PID parameter values of the conventional PSMC. Thus, APSMC is able to improve the tracking performance of the PSMC and guarantee the compliance, that is, safety. The synchronization between the ankle joint profile reference and the gait cycle is paramount for providing appropriate assistance. For this reason, an online adaptive reference trajectory is also proposed as a function of the walking speed of the wearer. This adaptive reference allows for an automatic synchronization between the wearer gait and the desired trajectory.

The tracking experiments with the online generated reference ankle joint trajectory have been carried out to prove the efficiency of the proposed method compared to the PSMC. The safety aspects of APSMC have been also evaluated by tracking experimentally a step signal input, which simulates a relative high tracking error. The experimental results show that APSMC provides better tracking performances with respect to the standard PSMC and at the same time is safer than PID controller.

References

1. J. A. Blaya, D. Newman and H. Herr, "Active Ankle Foot Orthoses (AAFO)," *Artificial Intelligence Laboratory*, Massachusetts Institute of Technology, Cambridge, MA (2002) pp. 275–277.
2. S. Hwang, J. Kim, J. Yi, K. Tae, K. Ryu and Y. Kim, "Development of an Active Ankle Foot Orthosis for the Prevention of Foot Drop and Toe Drag," *International Conference on Biomedical and Pharmaceutical Engineering (ICBPE)*, IEEE, Singapore (2006) pp. 418–423.
3. K. A. Shorter, J. Xia, E. T. Hsiao-Weckler, W. K. Durfee and G. F. Kogler, "Technologies for powered ankle-foot orthotic systems: Possibilities and challenges," *IEEE ASME Trans. Mechatron.* **18**(1), 337–347 (2013).
4. J. A. Blaya and H. Herr, "Adaptive control of a variable-impedance ankle-foot orthosis to assist drop-foot gait," *IEEE Trans. Neural Syst. Rehabil. Eng.* **12**(1), 24–31 (2004).
5. J. Hitt, A. M. Oymagil, T. Sugar, K. Hollander, A. Boehler and J. Fleeger, "Dynamically Controlled Ankle-foot Orthosis (DCO) with Regenerative Kinetics: Incrementally Attaining User Portability," *IEEE International Conference on Robotics and Automation (ICRA)*, IEEE, Roma, Italy (2007) pp. 1541–1546.
6. A. W. Boehler, K. W. Hollander, T. G. Sugar and D. Shin, "Design, Implementation and Test Results of a Robust Control Method for a Powered Ankle Foot Orthosis (AFO)," *IEEE International Conference on Robotics and Automation (ICRA)*, IEEE, Pasadena, CA, USA (2008) pp. 2025–2030.
7. M. Moltedo, T. Baček, K. Langlois, K. Junius, B. Vanderborcht and D. Lefeber, "Design and Experimental Evaluation of a Lightweight, High-torque and Compliant Actuator for an Active Ankle Foot Orthosis," *IEEE International Conference on Rehabilitation Robotics (ICORR)*, IEEE, London, UK (2017) pp. 283–288.
8. J. A. Ward, J. Hitt, T. Sugar and K. Bharadwaj, "Dynamic Pace Controller for the Robotic Gait Trainer," *International Design Engineering Technical Conferences and Computers and Information in Engineering Conference*, IDETC-CIE (2006), ASME, Pennsylvania, USA (2006) pp. 575–581.
9. D. P. Ferris, K. E. Gordon, G. S. Sawicki and A. Peethambaran, "An improved powered ankle-foot orthosis using proportional myoelectric control," *Gait Posture* **23**(4), 425–428 (2006).
10. K. A. Shorter, G. F. Kogler, E. Loth, W. K. Durfee and E. T. Hsiao-Weckler, "A portable powered ankle-foot orthosis for rehabilitation," *J. Rehabil. Res. Dev.* **48**(4), 459–472 (2011).
11. P. K. Jamwal, S. Q. Xie, S. Hussain and J. G. Parsons, "An adaptive wearable parallel robot for the treatment of ankle injuries," *IEEE/ASME Trans. Mechatron.* **19**(1), 64–75 (2014).
12. Y. Ren, Y.-N. Wu, C.-Y. Yang, T. Xu, R. Harvey and L.-Q. Zhang, "Developing a wearable ankle rehabilitation robotic device for in-bed acute stroke rehabilitation," *IEEE Trans. Neural Syst. Rehabil. Eng.* **25**(6), 589–596 (2016).
13. V. Arnez-Paniagua, H. Rifai, Y. Amirat and S. Mohammed, "Adaptive Control of an Actuated-Ankle-Foot-Orthosis," *IEEE International Conference on Rehabilitation Robotics (ICORR)*, IEEE, London, UK (2017) pp. 1584–1589.
14. M. N. A. Ab Patar, A. F. Said, J. Mahmud, A. P. A. Majeed and M. A. Razman, "System Integration and Control of Dynamic Ankle Foot Orthosis for Lower Limb Rehabilitation," *IEEE International Symposium on Technology Management and Emerging Technologies (ISTMET)*, IEEE, Bandung, Indonesia (2014) pp. 82–85.
15. V. Arnez-Paniagua, W. Huo, I. Colorado-Cervantes, S. Mohammed and Y. Amirat, "A Hybrid Approach Towards Assisting Ankle Joint of Paretic Patients," *International Functional Electrical Stimulation Society Conference (IFESS) (2016)*, La Grande-Motte, France (2016) pp. 1–4.
16. J. C. Pérez-Ibarra and A. A. G. Siqueira, "Comparison of Kinematic and EMG Parameters between Unassisted, Fixed-and Adaptive-stiffness Robotic-assisted Ankle Movements in Post-stroke Subjects," *International Conference on Rehabilitation Robotics (ICORR)*, IEEE, London, UK (2017) pp. 461–466.

17. F. el Zahraa Wehbi, W. Huo, Y. Amirat, M. El Rafei, M. Khalil and S. Mohammed, "Active Impedance Control of a Knee-joint Orthosis during Swing Phase," *IEEE International Conference on Rehabilitation Robotics (ICORR)*, IEEE, London, UK (2017) pp. 435–440.
18. M. J. Lawn, M. Takashima, M. Ninomiya, J. Yu, K. Soma and T. Ishimatsu, "Development of an actuation system for a rotary hydraulic brake on a low cost light weight knee-ankle-foot orthosis," *IEEE Sensors*, 1–4 (2015).
19. A. Roy, H. I. Krebs, K. Iqbal, N. R. Macko, R. F. Macko and L. W. Forrester, "Facilitating Push-off Propulsion: A Biomechanical Model of Ankle Robotics Assistance for Plantarflexion Gait Training in Stroke," *IEEE International Conference on Biomedical Robotics and Biomechatronics*, IEEE, Sao Paulo, Brazil (2014) pp. 656–663.
20. H. Rifai, S. Mohammed, W. Hassani and Y. Amirat, "Nested saturation based control of an actuated knee joint orthosis," *Mechatronics* **23**(8), 1141–1149 (2013).
21. B. Brahmi, M. Saad, C. Ochoa-Luna and M. H. Rahman, "Adaptive Control of an Exoskeleton Robot with Uncertainties on Kinematics and Dynamics," *International Conference on Rehabilitation Robotics (ICORR)*, IEEE, London, UK (2017) pp. 1369–1374.
22. M. Zhang, J. Cao, S. Q. Xie, G. Zhu, X. Zeng, X. Huang and Q. Xu, "A preliminary study on robot-assisted ankle rehabilitation for the treatment of drop foot," *J. Intell. Robot. Syst.* **91**(2), 1–9 (2017).
23. K. Bharadwaj, T. G. Sugar, J. B. Koeneman and E. J. Koeneman, "Design of a robotic gait trainer using spring over muscle actuators for ankle stroke rehabilitation," *J. Biomech. Eng.* **127**(6), 1009–1013 (2005).
24. W. Huo, S. Mohammed, J. C. Moreno and Y. Amirat, "Lower limb wearable robots for assistance and rehabilitation: A state of the art," *IEEE Syst. J.* **10**(3), 1068–1081 (2016).
25. J. Ward, T. Sugar, J. Standeven and J. R. Engsborg, "Stroke Survivor Gait Adaptation and Performance after Training on a Powered Ankle Foot Orthosis," *International Conference on Robotics and Automation (ICRA)*, IEEE, Anchorage, Alaska (2010) pp. 211–216.
26. I. Veneva and N. Ferreira, "Adaptive System for Control of Active Ankle-foot Orthosis and Gait Analysis," *In: Mathematical Methods in Engineering* (Springer, Dordrecht, 2014) pp. 153–163.
27. V. Arnez-Paniagua, H. Rifai, Y. Amirat and S. Mohammed, "Adaptive Control of an Actuated-Ankle-Foot-Orthosis," *International Conference on Rehabilitation Robotics (ICORR)*, IEEE, London, UK (2017) pp. 1584–1589.
28. R. Jiménez-Fabián and O. Verlinden, "Review of control algorithms for robotic ankle systems in lower-limb orthoses, prostheses, and exoskeletons," *Med. Eng. Phys.* **34**(4), 397–408 (2012).
29. S. M. Cain, K. E. Gordon and D. P. Ferris, "Locomotor adaptation to a powered ankle-foot orthosis depends on control method," *J. Neuroeng. Rehabil.* **4**(1), 1 (2007).
30. M. Van Damme, B. Vanderborght, B. Verrelst, R. Van Ham, F. Daerden and D. Lefeber, "Proxy-based sliding mode control of a planar pneumatic manipulator," *Int. J. Rob. Res.* **28**(2), 266–284 (2009).
31. J. Huang, Z.-H. Guan, T. Matsuno, T. Fukuda and K. Sekiyama, "Sliding-mode velocity control of mobile-wheeled inverted-pendulum systems," *IEEE Trans. Rob.* **26**(4), 750–758 (2010).
32. B. Yao and M. Tomizuka, "Adaptive robust control of SISO nonlinear systems in a semi-strict feedback form," *Automatica* **33**(5), 893–900 (1997).
33. R. Kikuuwe and H. Fujimoto, "Proxy-based Sliding Mode Control for Accurate and Safe Position Control," *IEEE International Conference on Robotics and Automation (ICRA)*, IEEE, Orlando, Florida (2006) pp. 25–30.
34. M. Huang, X. Huang, X. Tu, Z. Li and Y. Wen, "An online gain tuning proxy-based sliding mode control using neural network for a gait training robotic orthosis," *Cluster Comput.* **19**(4), 1987–2000 (2016).
35. B. Badreddine, A. Zaremba, J. Sun and F. Lin, "Active damping of engine idle speed oscillation by applying adaptive pid control," Technical report, SAE Technical Paper (2001).
36. E. Hutin, D. Pradon, F. Barbier, B. Bussel, J.-M. Gracies and N. Roche, "Walking velocity and lower limb coordination in hemiparesis," *Gait Posture* **36**(2), 205–211 (2012).
37. R. Kikuuwe, S. Yasukouchi, H. Fujimoto and M. Yamamoto, "Proxy-based sliding mode control: A safer extension of pid position control," *IEEE Trans. Rob.* **26**(4), 670–683 (2010).
38. C. Barbalata, V. De Carolis, M. W. Dunnigan, Y. Petillot and D. Lane, "An Adaptive Controller for Autonomous Underwater Vehicles," *IEEE/RSJ International Conference on Intelligent Robots and Systems (IROS)*, Hamburg, Germany (2015) pp. 1658–1663.
39. R. D. Brandt and F. Lin, "Adaptive interaction and its application to neural networks," *Inf. Sci.* **121**(3–4), 201–215 (1999).
40. B. M. Badreddine and F. Lin, "Adaptive PID Controller for Stable/unstable Linear and Non-linear Systems," *IEEE International Conference on Control Applications (CCA)*, IEEE, Mexico City, Mexico (2001) pp. 1031–1036.
41. Z.-Y. Zhao, M. Tomizuka and S. Isaka, "Fuzzy gain scheduling of pid controllers," *IEEE Trans. Syst. Man Cybern.* **23**(5), 1392–1398 (1993).
42. H. Rifai, S. Mohammed, B. Daachi and Y. Amirat, "Adaptive Control of a Human-driven Knee Joint Orthosis," *IEEE International Conference on Robotics and Automation (ICRA)*, St. Paul, Minnesota, USA (2012) pp. 2486–2491.